A Theoretical Model for Computing Freezing Point Depression of Lithium-Ion Battery Electrolytes

To cite this article before publication: Julian Self *et al* 2021 *J. Electrochem. Soc.* in press https://doi.org/10.1149/1945-7111/ac3e47

A Theoretical Model for Computing Freezing Point Depression of Lithium-Ion Battery Electrolytes

Journal:	*Journal of The Electrochemical Society*
Manuscript ID	JES-105690.R1
Manuscript Type:	Research Paper
Date Submitted by the Author:	22-Oct-2021
Complete List of Authors:	Self, Julian; Lawrence Berkeley National Laboratory, Energy Technologies Area Bergstrom, Helen; University of California Berkeley, Chemical & Biomolecular Engineering Fong, Kara; University of California Berkeley, Chemical & Biomolecular Engineering Mccloskey, Bryan; University of California, Berkeley, Chemical and Biomolecular Engineering Persson, Kristin A.; Lawrence Berkeley National Laboratory, Energy Technologies Area
Keywords:	Batteries – Li-ion, Thermodynamics, Theory and Modelling

A Theoretical Model for Computing Freezing Point Depression of Lithium-ion Battery Electrolytes

Julian Self,[†,‡] Helen K. Bergstrom,[‡,¶] Kara D. Fong,[‡,¶] Bryan D. McCloskey,[‡,¶] and Kristin A. Persson[*,†,‡,§]

†*Department of Materials Science and Engineering, University of California, Berkeley*

‡*Energy Technologies Area, Lawrence Berkeley National Laboratory*

¶*Department of Chemical and Biomolecular Engineering, University of California, Berkeley*

§*The Molecular Foundry, Lawrence Berkeley National Laboratory*

E-mail: kapersson@lbl.gov

November 29, 2021

Abstract

Reliable prediction of freezing point depression in liquid electrolytes will accelerate the development of improved Li-ion batteries which can operate in low temperature environments. In this work we establish a computational methodology to calculate activity coefficients and liquidus lines for battery-relevant liquid electrolytes. Electronic structure methods are used in conjuction with classical molecular dynamics simulations and theoretical expressions for Born solvation energy, ion-atmosphere effects from Debye-Hückel theory and solvent entropic effects. The framework uses no a priori knowledge beyond neat solvent properties and the concentration of salt. $LiPF_6$ in propylene carbonate (PC), $LiPF_6$ in dimethyl carbonate (DMC) and $LiClO_4$ in

DMC are investigated up to 1 molal with accuracy better than 3°C when compared to experimental freezing point measurements. We find that the difference in freezing point depression between the propylene carbonate-based electrolyte and the dimethyl cabonate electrolytes originates from the difference in the solvent dielectric constant.

Introduction

The importance of phase equilibria for lithium ion battery (LIB) electrolytes is well known.[1–12] Phase behavior, as described by phase diagrams, helps determine the operating windows of liquid electrolytes. Recently, there is a significant effort devoted to extending the viability of LIB to lower temperatures (T),[13,14] and as such knowledge of the exact freezing point of liquid electrolytes is pertinent. Moreover, the freezing point depression is directly related to fundamental thermodynamics and the physical chemistry of liquid electrolytes through the activity coefficients, which affect electrochemical stability and transport behaviour. In this work we develop a methodology to obtain the freezing point depression and activity coefficients of LIB-relevant electrolytes from computational methods for concentrations up to 1 molal (m). We undertake case studies for three systems of interest: $LiPF_6$ in propylene carbonate (PC), $LiClO_4$ in dimethyl carbonate (DMC), and $LiPF_6$ in DMC. These systems are chosen as the two solvents are significantly different in nature (low vs. high permittivity and linear vs. cyclic) and there is significant thermodynamic data already published to compare our results to.

Kinetics of charge transfer as well as bulk transport in electrodes and in electrolytes are a concern at low temperature.[15–17] In this work we specifically focus on challenges associated with bulk transport in the electrolyte at low temperatures. In order to maintain sufficient conductivity, it is essential that the electrolyte of use remains in liquid phase, i.e. does not freeze[17] — motivating this work. If we consider the low temperature range necessary for deployment of LIBs in cold climates from -40°C to 25°C, then conventionally-used ternary electrolytes[11] are inadequate as they generally show freezing at ∼-20°C.[1,17,18] Freezing point

depression, θ, is the difference in the freezing point of the neat solvent and that of the electrolyte. In a binary, single-solvent electrolyte θ can be computed from the solvent activity a_{solvent}, knowing neat solvent properties such as the freezing temperature T_0, the enthalpy of fusion $\Delta\overline{H}_{\text{fus}}$ and the difference in heat capacity between the two phases Δc_P, with the gas constant denoted as R:[19]

$$\theta = \frac{\Delta\overline{H}_{\text{fus}} - 2RT_0 \ln a_{\text{solvent}} - \sqrt{2\Delta c_P {T_0}^2 R \ln a_{\text{solvent}} + \Delta\overline{H}_{\text{fus}}^2}}{2\Delta\overline{H}_{\text{fus}}/T_0 + \Delta c_P - 2R \ln a_{\text{solvent}}} \,. \tag{1}$$

In the above equation, $\Delta\overline{H}_{\text{fus}}$ and Δc_P are assumed constant as a function of temperature.

Herein, we first discuss theoretical schemes to compute salt activity coefficients, which are directly related to the solvent activity, a_{solvent}.[20] Ideal solutions, Debye-Hückel theory,[20–22] Pitzer-type models,[23–27] and the mean spherical approximation[28,29] (MSA), are discussed. We then propose an alternative approach, which involves Debye-Hückel theory augmented with Born solvation,[30–32] ion pairing[29] and solvent entropic effects related to the free solvent fraction.[33] We present methodology to obtain the ionic radii[34] and concentration-dependent dielectric constant,[35] which are input parameters used in our proposed theoretical approach. The obtained thermodynamic properties, used in conjunction with neat solvent properties, allow calculation of liquidus lines in the phase diagrams which are compared to experimental measurements.

Salt activity coefficients

Various models may be used to compute the molal salt activity coefficient, $\gamma_{\pm}$, which, for 1-1 electrolytes, appears in the expression for the chemical potential of the salt in solution (denoted μ_{salt}, with the infinite dilution salt reference state denoted as μ^0_{salt}) as follows:

$$\mu_{\text{salt}} - \mu^0_{\text{salt}} = 2RT\ln(\gamma_{\pm} m) \tag{2}$$

In the simplest case, we can assume ideality ($\gamma_{\pm} = 1$), implying there are no interactions

between species in solution. In this case, equation 2 simplifies to the following:

$$\mu_{\text{salt}} - \mu^0_{\text{salt}} = 2RT\ln(m) \tag{3}$$

The Debye-Hückel (DH) theory of electrolyte solutions considers the change in the chemical potential of an ion in solution due to the ionic environment,[20,22] where the molality of positive and negative ions are written as m_- and m_+ :

$$\mu_{\text{salt}} - \mu^0_{\text{salt}} = RT\ln(\gamma_{\text{DH},+}) + RT\ln(\gamma_{\text{DH},-}) + RT\ln(m_+) + RT\ln(m_-) \tag{4}$$

DH theory accounts for ion-ion interactions via a mean field approach where the Poisson-Boltzmann equation is linearized.[20,22] When used alone, DH theory assumes full dissociation of ions. An analytic DH solution exists, and the DH activity coefficient $\gamma_{\text{DH},i}$ can be explicitly written as follows, with z_i as species charge:[20,34]

$$\ln\gamma_{\text{DH,i}} = -z_i^2 \frac{A_{\text{DH}}\sqrt{I}}{1 + B_{\text{DH}}\alpha_{\text{DH}}\sqrt{I}} \tag{5}$$

DH theory predicts a decrease of $\gamma_{\text{DH},i}$ with increasing ionic strength (i.e. as we add salt). The molal ionic strength, I, is defined via the following expression:

$$I = 0.5\sum_i z_i^2 m_i \tag{6}$$

The DH term B_{DH} is defined by the following expression, where F is Faraday's constant, ε_0 is the electric constant, ε is the permittivity, and ρ_0 the neat solvent density:

$$B_{\text{DH}} = \frac{F}{(\varepsilon_0\varepsilon RT/2)^{0.5}}\sqrt{\rho_0} \tag{7}$$

α_{DH} is the distance of closest approach between ions,[34] e.g. the sum of radii of cation and anion species. The DH parameter A_{DH} can be expressed via the following relationship, where the units are the square root of inverse molality, allowing A_{DH} to often be expressed

as unitless provided the ionic strength is also in units of molality. An expression for A_{DH} is as follows, where e is the elementary charge:

$$A_{\mathrm{DH}} = \frac{Fe}{8\pi\varepsilon_0\varepsilon RT} B_{\mathrm{DH}} \tag{8}$$

At sufficiently high concentrations (e.g. above 0.01 m), DH theory alone is insufficient to account for all non-idealities due to, among many factors, changes in permittivity, changes in specific ion-ion and ion-solvent interactions (e.g. ion pairing).[22,36] Empirically, this can be accounted for via a Guggenheim-type equation:[20,37,38]

$$\ln\gamma_{\mathrm{Gugg},i} = \ln\gamma_{\mathrm{DH},i} + B_{\mathrm{K}} I + C_{\mathrm{K}} I^{3/2} \tag{9}$$

However, the exact physical origins of B_{K} and C_{K} are unspecified and as such these coefficients cannot be calculated a priori. Similar to the Guggenheim-type expression, the Pitzer equations are widely used semi-empirical expressions for the activity of aqueous and non-aqueous electrolytes.[24–27] The equations are as follows:

$$\ln(\gamma_{\pm}) = \frac{-A^{\phi}\sqrt{I}}{1+b\sqrt{I}} - \frac{2A^{\phi}}{b}\ln(1+b\sqrt{I}) + mB^{\gamma} + \frac{3}{2}m^2 C^{\phi} \tag{10}$$

$$B^{\gamma} = 2\beta^{(0)} + \xi^{(1)} + \xi^{(2)} \tag{11}$$

$$\xi^{(i)} = \frac{2\beta^{(i)}}{\alpha_i^2 I}[1 - (1 + \alpha_i\sqrt{I} - \frac{1}{2}\alpha_i^2 I)\exp(-\alpha_i\sqrt{I})] \tag{12}$$

$$A^{\phi} = \frac{A_{\mathrm{DH}}}{3} \tag{13}$$

Seven parameters must be adjusted: b, $\beta^{(0)}$,$\beta^{(1)}$, $\beta^{(2)}$, α_1, α_2 and C^{ϕ}. Generally, all seven of these parameters cannot be predicted a priori. Moreover, often in calculating the ionic

strength, it is assumed that there is no ion pairing and the concentration of charged species is the same as the concentration of the salt.[26,27] Especially in low permittivity media, this assumption is incorrect and the Pitzer-type model is implicitly fit to experimental data via unreasonably large ionic radii. For example, we can identify b with $B_{\mathrm{DH}}\alpha_{\mathrm{DH}}$ where B_{DH}=16.52 nm^{-1} and b has been reported as 95 for DMC-based electrolytes,[27,39] implying α_{DH}=5.75 nm. This value is unreasonably large and the parameter b is arguably used to mask the shortcomings of the Pitzer-type model at accounting for long-range electrostatics. This is discussed further below. A theoretical alternative to the Guggenheim-type and Pitzer-type models is the MSA,[28,29,40–42] which builds on DH-theory in that the ions' radii now contribute to an additional volume exclusion term to the chemical potential. However, MSA by itself does not account for the effects of the concentration-dependent change in permittivity of electrolytes, which is known to be important especially in low permittivity electrolytes.[43] Some scholarship has allowed for MSA enhanced with consideration of concentration-dependent permittivity effects,[44,45] although with many adjustable parameters, which may not be obtainable a priori. Thus, since the MSA either uses many adjustable parameters or does not account for concentration-dependent permittivity effects, it is herein avoided. Moreover, the work presented here is suggested as an alternative to theories with adjustable parameters, while both capturing the important underlying physical chemistry in solution and predicting thermodynamics properties with reasonable accuracy.

Theory

In this work we propose to account for non-idealities with consideration of Born solvation, ion pairing effects and free solvent number, in addition to DH theory. This departs from Pitzer and MSA models which, when applied alone, ignore Born solvation and free solvent effects. DH theory accounts for long-range ion-ion interactions between all charged species. Born solvation accounts for long-range ion-solvent interactions via the dielectric medium of the electrolyte created by the solvent molecules and polar associated salt species (e.g. ion

pairs). Ion pairing[29] accounts for specific, short-range, ion-ion interactions. Ion pairs are formed when closely interacting ions form a single kinetic entity, i.e. move together for an appreciable amount of time.[29] These may be unimportant in certain aqueous electrolytes due to the high dielectric constant of the aqueous solvent, but ion pairing generally becomes more important as the polarity of the solvent decreases. For example, in low permittivity solvents ($\varepsilon < 10$), ion pairing may be significant even in the semi-dilute regime.[29,43] The simplest 1-1 electrolyte ion pairing equilibrium involves species, S, of free ions S_+, S_- and contact-ion pairs (CIP), S_{CIP}:

$$S_+ + S_- \rightleftharpoons S_{\text{CIP}} \tag{14}$$

In lithium-salt carbonate-solvent electrolytes, the solvent and cation interact very strongly, such that the cation and its full solvation shell form long-lived clusters.[46] Thus, in this work, cations are considered with their primary solvation shell, which is assumed to hold a fixed number of solvent molecules. Moreover, we will account for the entropic losses that result upon free solvent binding to cations, as well as the entropic gains from solvent molecules released upon ion pairing. If a cation, via its primary solvation shell, is bound to $n_{\text{s},+}$ solvent molecules S_0 and the CIP to $n_{\text{s,CIP}}$ solvent molecules, the ion-pairing equilibrium can be written as follows:

$$\left((S_0)_{n_{\text{s},+}} S_+\right) + S_- \rightleftharpoons \left((S_0)_{n_{\text{s,CIP}}} S_{CIP}\right) + (n_{\text{s},+} - n_{\text{s},CIP}) S_0 \tag{15}$$

For the above equilibrium, we can denote the infinite dilution association constant $K_{\text{A}}^0 = \exp(-\Delta G_{\text{A}}^0/RT)$, where G_{A}^0 is the free energy change upon ion pairing, as in equation 15. We note that there may be equilibria with higher order associated species and aggregates,[29] which are not considered in this work but would likely be necessary for investigations of concentrations above 1 m in Li-ion electrolytes. For a fraction of free ions α, we can establish the following:

$$\mu_{\text{salt}} - \mu^0_{\text{salt}} = \alpha\mu_+ + \alpha\mu_- + (1-\alpha)\mu_{\text{CIP}} \tag{16}$$

We can write the expression for the individual contributions to the chemical potential of free ions as the following, where $\gamma_{\text{B},i}$ refers to the Born solvation contribution to the activity coefficient, and $\gamma_{\text{FSL},i}$ the entropic contribution from free solvent loss:

$$\mu_+ - \mu^0_+ = RT\ln(\gamma_{\text{DH},+}) + RT\ln(\gamma_{\text{B},+}) + RT\ln(\gamma_{\text{FSL},+}) + RT\ln(m_+) \tag{17}$$

Similarly, for the anion, we can write:

$$\mu_- - \mu^0_- = RT\ln(\gamma_{\text{DH},-}) + RT\ln(\gamma_{\text{B},-}) + RT\ln(m_-) \tag{18}$$

Explicitly, the Born solvation expression[31,32] is:

$$\ln(\gamma_{\text{B},i}) = \frac{e^2}{8\pi\varepsilon_0 R_{\text{B},i} RT}\left(\frac{1}{\varepsilon(m)} - \frac{1}{\varepsilon(m=0)}\right) \tag{19}$$

In the above equation $R_{\text{B},i}$ is the Born radius. Accordingly, for an ion of a fixed radius $R_{\text{B},i}$, its free energy is lowered if the medium it is dissolved in incurs an increase in dielectric constant. The third term on the right-hand side of equation 17 is relevant to the entropy loss of free solvent molecules from formation of cation solvation shells. For a species which binds solvent molecules (e.g. cations or CIPs), the chemical potential contribution from the loss in free solvent entropy from the creation of the solvation shell can be written as:[47]

$$\ln(\gamma_{\text{FSL,i}}) = -n_{\text{s,i}}\ln(\frac{m_{\text{free solvent}}}{m_{\text{solvent}}}) \tag{20}$$

where $m_{\text{free solvent}}$ is the molality of free solvent, which, at infinite dilution, is equal to the neat solvent molality ($m^0_{\text{free solvent}} = m_{\text{solvent}}$, see Supplemental Information for further details). In this work it is assumed anions do not bind solvent molecules (vide infra). The free solvent molality can be calculated knowing the concentration of species and the solvation numbers

$n_{s,+}$ and $n_{s,CIP}$:

$$m_{\text{free solvent}} = m_{\text{solvent}} - m_{+}n_{s,+} - m_{CIP}n_{s,CIP} \tag{21}$$

In equation 16 the chemical potential of the CIP μ_{CIP} is:

$$\mu_{CIP} = -RT\ln(K_A^0) + RT\ln(\gamma_{FSL,CIP}) + RT\ln(m_{CIP}) \tag{22}$$

The first term accounts for the fact that the reference state is that of free ions at infinite dilution, where all free ion and CIP activity coefficients are set to $\gamma_i = 1$.

α, which appears in equation 16, is related to the concentration equilibrium constant K_A, defined via the following mass action law:[29]

$$K_A = \frac{m_{CIP}}{m_{+}m_{-}} = \frac{1-\alpha}{\alpha^2 m} \tag{23}$$

We can also relate the concentration equilibrium constant K_A to K_A^0 via:[29]

$$K_A = K_A^0 \frac{\gamma_{DH,+}\gamma_{B,+}\gamma_{FSL,+}\gamma_{DH,-}\gamma_{B,-}}{\gamma_{FSL,CIP}} \tag{24}$$

Accordingly, K_A^0 is concentration independent and is related to the concentration equilibrium constant via the relevant activity coefficients.[29]

A combination of equations 16, 17, 18 and 22 provides an expression for the chemical potential as a function of the fraction of species and the various activity coefficients:

$$\mu_{salt} - \mu_{salt}^0 = RT\left(\frac{m_{+}}{m}\ln(\gamma_{B,+}\gamma_{DH,+}\gamma_{FSL,+}m_{+}) + \frac{m_{-}}{m}\ln(\gamma_{B,-}\gamma_{DH,-}m_{-}) + \frac{m_{CIP}}{m}\ln(\frac{\gamma_{FSL,CIP}m_{CIP}}{K_A^0})\right) \tag{25}$$

The quantity of interest, the experimentally accessible $\gamma_{\pm}$, is directly related to the chemical potential of the salt via arrangement of equation 2:

$$\gamma_{\pm} = \frac{1}{m}\exp\left(\frac{\mu_{\text{salt}} - \mu^0_{\text{salt}}}{2RT}\right) \tag{26}$$

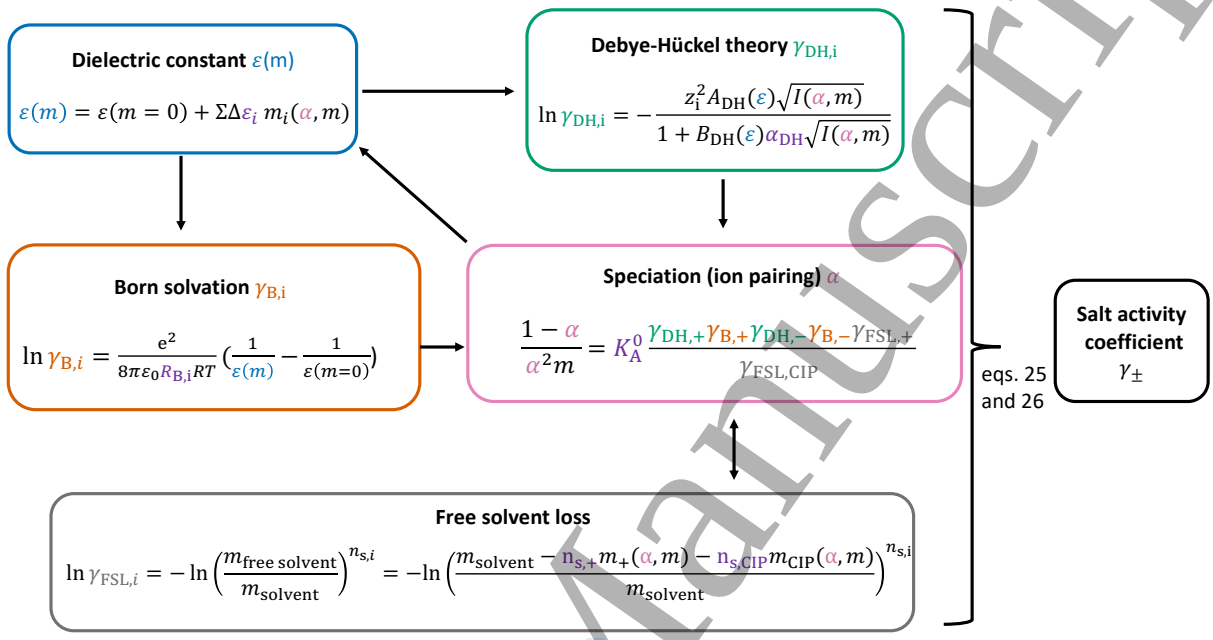

Figure 1: Schematic on methodology to compute the salt activity coefficient in the present work. Input parameters which are computed a priori and are not dependent on molality are shown in purple. We note $\alpha_{\text{DH}} = R_{\text{B},+} + R_{\text{B},-}$. The various theories employed (DH, Born solvation and ion pairing) are interdependent, as shown by arrows, and are also interdependent with the dielectric constant. Various quantities of interest are color-coded for visual ease. We further note $\alpha = \frac{m_+}{m} = \frac{m_-}{m} = \frac{m - m_{\text{CIP}}}{m}$.

Figure 1 shows a schematic on the methodology to compute the salt activity coefficient $\gamma_{\pm}$ in the present work. The parameters that are not dependent on molality and that are computed via electronic structure methods or molecular dynamics simulations are shown in purple. In the scheme proposed in this work, $\gamma_{\pm}$ can be calculated via equations 5, 19, 20, 23, 25 and 26, and with knowledge of K^0_{A}, $\varepsilon(m)$, the values of $n_{\text{s},i}$, $R_{\text{B},i}$ and $\alpha_{\text{DH},i}$. Since these latter quantities will be computed using either electronic structure or classical molecular dynamics methods, with no a priori experimental knowledge of the physical effects of salt on the electrolyte, we distinguish the herein used methodology from Pitzer-type models, which use adjustable parameters. Although the liquid electrolytes concepts of DH theory, Born solvation, ion pairing and free solvent number are well-known, to the authors' knowledge

they have not been previously used together to obtain the chemical potential of species in a computational context. Presumably this is due to the difficulties of obtaining the concentration-dependent dielectric constant of the electrolyte.

Input parameters to model

The radii of ions $R_{\mathrm{B},i}$ and ionic distance of closest approach α_{DH}, as appearing in equations 5 and 19, are parameters that are used in the Born solvation theory and DH theory, respectively. In this work the DH distance α_{DH} is picked as the sum of the two relevant Born radii:

$$\alpha_{\mathrm{DH}} = (R_{\mathrm{B},+} + R_{\mathrm{B},-}) \tag{27}$$

There are many approaches that can be used to obtain radii, either α_{DH} and/or $R_{\mathrm{B},i}$, for example, the experimental ionic radii (e.g. from solid salt crystals),[48,49] the experimental molar conductivity as a function of molar salt concentration $\Lambda(c)$,[43] the experimental activity coefficient $\gamma_{\pm}(c)$,[27,39] the experimental solvation energy $\Delta G_i^{\mathrm{s}}(\varepsilon)$[50] and the computed solvation energy $\Delta G_i^{\mathrm{s}}(\varepsilon)$.

Various radii are shown in Table 1. There is no exact measure of radii in both DH theory and the Born theory of solvation.[34] Generally, it is accepted that that the relevant measure of radii in solution should be somewhere between the "bare" ionic radii and the size of a solvated ion-cluster.[22] As expected, the crystallographic ("bare") ionic radii[52] shown in Table 1 are the smallest. For $LiClO_4$ and $LiAsF_6$ in DMC, the Born radii fit to molar conductivity (i.e. the conductivity normalized by salt concentration), $\Lambda(c)$, data have been reported. For these reported values, DH effects were neglected ($\gamma_{\mathrm{DH},i} = 1$) and, $R_{\mathrm{B},i}$ and K_{A}^0 were simultaneously fit with the $\Lambda(c)$ data.[43] We show the reported values for AsF_6^- as they are likely representative to those of PF_6^- due to similar chemical structure and formula. Here, due to the investigators' inherent inability to decouple the activity coefficients of the anion and cation from fitting $\Lambda(c)$, the ions' radii are in effect equal. For the present work, we desire a methodology to obtain radii which does not require a priori experimental data,

Table 1: Radii and solvation number of ionic species obtained via various methods. PW refers to values computed and used in the present work.

	Radius	Notes	ref.
R_{Li}	0.076 nm	crystallographic radius	[51]
R_{PF6}	0.254 nm	crystallographic radius	[51]
R_{ClO4}	0.236 nm	crystallographic radius	[51]
$R_{\mathrm{B,Li}}$(PC)	0.16 nm	from ΔG^{s} (Comp.)	PW
$R_{\mathrm{B,Li}}$(DMC)	0.40 nm	from ΔG^{s} (Comp.)	PW
$R_{\mathrm{B,PF6}}$(DMC)	0.31 nm	from ΔG^{s} (Comp.)	PW
$R_{\mathrm{B,PF6}}$(PC)	0.31 nm	from ΔG^{s} (Comp.)	PW
$R_{\mathrm{B,ClO4}}$(DMC)	0.30 nm	from ΔG^{s} (Comp.)	PW
$R_{\mathrm{B,Li}}$(DMC) , $R_{\mathrm{B,AsF6}}$ (DMC)	0.63 nm	fit: Born, no DH from Λ(c)	[43]
$R_{\mathrm{B,Li}}$(DMC) , $R_{\mathrm{B,ClO4}}$ (DMC)	0.58 nm	fit: Born, no DH from Λ(c)	[43]
$R_{\mathrm{B,Li}}$(DMC) , $R_{\mathrm{B,ClO4}}$ (DMC)	3 nm	fit: Pitzer $\gamma_{\pm}$(m)	[39]
$R_{\mathrm{B,Li}}$(DMC) , $R_{\mathrm{B,PF6}}$ (DMC)	3 nm	fit: Pitzer $\gamma_{\pm}$(m)	[27]
	Solvation Number		
$n_{\mathrm{s},+}$ (Li^+ in PC)	6	from MD	PW
$n_{\mathrm{s,CIP}}$ ($LiPF_6$ in PC)	5	from MD	PW
$n_{\mathrm{s},+}$ (Li^+ in DMC)	5	from MD	PW
$n_{\mathrm{s,CIP}}$ ($LiPF_6$ in DMC)	4	from MD	PW
$n_{\mathrm{s,CIP}}$ ($LiClO_4$in DMC)	4	from MD	PW

precluding for example the use of molar conductivity-obtained ionic radii. Here, the radii $R_{\mathrm{B},i}$ are solved for via the calculation of a change in the free energy of solvation ΔG_i^{s}, using the following equation:[50]

$$\Delta G_i^{\mathrm{s}}(m \to 0) = \frac{e^2}{8\pi\varepsilon_0 R_{\mathrm{B},i}}\left(\frac{1}{\varepsilon_2(m=0)} - \frac{1}{\varepsilon(m=0)}\right) \tag{28}$$

Here, ΔG_i^{s} calculates the free energy change of a species solvated in solution as the dielectric constant changes from ε to ε_2. For Li^+ in DMC, $R_{\mathrm{B,Li}}$=0.40 nm was found via use of equation 28 and electronic structure methods. For cations, the first solvation shell was included in the electronic structure calculations, in addition to a continuum solvation model[53] (further details in Computational Methods). The value obtained for Li^+ in DMC is about five times larger than the "bare" ionic radii but closer to the experimental value fit from $\Lambda(c)$ data. The anions's radii were calculated in a similar fashion, in this case without an explicit first solvation shell as anion-solvent short range interactions are approximated here as negligible.[42,54] We note that preferential solvation of cations over anions is an active research topic.[55] As expected, the values for PF_6^- found were very close to the "bare" ionic radii. For the PC electrolyte system, the computed PF_6^- anion radius was identical as for the DMC system (0.31 nm). For Li^+, the radius value is smaller for the PC system (0.16 nm vs 0.40 nm for the DMC case). Although no analogous literature values for Born radii were found for Li^+ and PF_6^- in PC, a previous publication reported a value of 1.5 Å for Li^+ in water,[50] which holds a comparable dielectric constant to PC. As discussed previously, using a Pitzer-model approach, the ionic radii obtained for DMC electrolytes are unreasonably overestimated, where the radii are those which are implicitly used in the DH term of the Pitzer-type equations ($R_{\mathrm{B,Li}} \sim \alpha_{\mathrm{DH,Li}}/2$). For example, the values for the Li^+-in-DMC radii with a Pitzer-type model are an order of magnitude larger than the size of the solvation shell,[26,27] and two orders of magnitude larger than the Li^+ crystallographic radius. Moreover, this is likely due to overfitting of the model — and more precisely, the lack of Born solvation (i.e. concentration-dependent permittivity effects) in the Pitzer model. This suggests that

the use of the Pitzer-type equations to fit thermodynamic data of non-aqueous electrolytes may be more analogous to polynomial fitting than to a rigorous underlying theory. The computed solvation numbers ($n_{s,i}$ values between 4 and 6), listed in Table 1, are in general agreement with previous reports.[46,56–61] Sample solvation structures obtained from MD are shown in Figure S1.

In the current work, the concentration dependent dielectric constant, which is needed to compute equations 5 and 19, requires knowledge of the speciation (e.g. the molality of each species m_i) and dielectric increment per species $\Delta\varepsilon_i$ and is calculated via the following:

$$\varepsilon(m) = \varepsilon(m=0) + \Sigma\Delta\varepsilon_i m_i \tag{29}$$

K^0_A, the $\Delta\varepsilon_i$ values, the $n_{s,i}$ values, the $R_{B,i}$ values, equations 5, 19, 20, 24, 27, 29 and the neat solvent dielectric constant (Table 2) were here used to simultaneously solve for speciation (m_i values) and $\varepsilon(m)$. The equations used form a system of non-linear coupled equations, in addition to the relationships for mass conservation and electroneutrality. Figure 1 shows the equations used in this methodology. A numerical approach to solve the non-linear coupled equations was developed with in-house code, available at https://github.com/JSelf42/FreezingPointDepression. Table 3 shows the values of K^0_A computed and used in this work, as well as the computed dielectric increment values. K^0_A values were computed from the above-described electronic structure calculations used for calculating the species' radii. Dielectric increment values were computed via classical molecular dynamic simulations (see Methods for further details). For the DMC systems, the computed K^0_A values are higher than experimental ones. We encourage caution in comparing against experimental results as the experimental K^0_A was obtained by simultaneously fitting the Born radii,[43] in this case neglecting DH effects. From equations (vide infra) 30 and 32, $\Delta\varepsilon_{CIP}$ is found to be considerably large and positive, reflecting the dipolar nature of CIP species. Similarly, $\Delta\varepsilon_i$ for free ions in DMC were found to slightly exceed zero, suggesting structure promotion. For the PC system, the computed K^0_A is in

excellent agreement with the reported experimental value. The cation $\Delta\varepsilon_i$ was found to be substantially negative (-44/m), which we attribute to the loss of free solvent molecules when PC molecules are bound in solvation shells (e.g. by the cation). Here, the positive CIP $\Delta\varepsilon_i$ reflects the significant dipole moment of the CIP. Once the speciation and dielectric constant are found as a function of concentration, equations 25 and 26 allow to solve for the (experimentally accessible) $\gamma_\pm$, which is directly related to the solvent activity via the Gibbs-Duhem relation.[20] The calculated solvent activities a_{solvent}, as well as reported neat solvent properties which are shown in Table 2, allow the calculation of the liquidus lines. The neat solvent properties used are the melting temperature, T_0, the enthalpy of fusion $\Delta\overline{H}_{\text{fus}}$, the change in heat capacity upon freezing Δc_P and the neat solvent density.[1,2] The relationships to obtain the liquidus from the solvent activity follow Ge and Wang,[19] as shown in equation 1.

In this work the activity coefficients are calculated at 25°C, which allows comparison to reported data. The assumption that follows is that the activity coefficients calculated at room temperature can be used to reasonably estimate the activity coefficients near the freezing temperature of the liquid electrolyte. Considering the temperature dependence of activity coefficients is left to further work.

Table 2: Experimental neat solvent properties used in this work. Bold values were measured in the present work.

Solvent	T_0 (C)	$\Delta\ \overline{H}_{\text{fus}}$ (kJ/mol)	Δc_P (J/mol K)	density (kg/L)	$\varepsilon(c=0)$	ref.
PC	-48.8	8.960	33	1.20	65	[1,2,62,63]
DMC	**4.3**	**12.36**	29	1.07	3.1	[1,2,43]

Table 3: Association constants and dielectric increment per salt species

System	K_A^0 (1/M,PW) PW	K_A^0 (1/M,exp) ref.[43,51]	$\Delta\varepsilon_{CIP}$(1/m) PW	$\Delta\varepsilon_+$(1/m) PW	$\Delta\varepsilon_-$(1/m) PW
DMC/$LiPF_6$	3.5×10^{16}	$8.9 \times 10^{11*}$	23	2.9	1.2
DMC/$LiClO_4$	1.8×10^{17}	$8.6 \times 10^{12*}$	17	2.9	1.2
PC/$LiPF_6$	2.0	2.1	11	-44	-22

* The thermodynamic assumptions used in fitting for this value from experiment[43] were significantly different than those used in the present work (see text).

Computational Methods

Association Constants, Radii and Solvation Numbers

Infinite dilution association constants K_A^0, shown in Table 3, were calculated via first-principles quantum chemistry methods of the free energy change relevant to equation 15. More specifically, hybrid DFT calculations were undertaken with Gaussian 016 software using the wb97x-d functional with the 6-31+g(d,p) basis set and a continuum solvation model (CSM)[53,64–66] using the neat solvent permittivity as well as an explicit solvation shell for cations (both free and in CIPs). Before geometry optimization via electronic structure methods, initial configurations were picked via conformational analysis using Macromodel and an OPLS-based force field, where structures with solvation numbers matching those from the classical MD simulations were picked. The latter were computed via analysis of the radial distribution function of species simulated via MD (vide infra). In order to correct for spurious contributions of low-frequency modes to the vibrational partition function for the electronic structure calculations, Truhlar's[67] correction was applied using the "GoodVibes" code package.[68] To obtain the Born radii of cations or anions, the continuum solvation model (i.e. PCM) dielectric constant was varied in the above-described calculations for free energy of species in solution, and the resulting energy change allowed calculation of the Born radius according to equation 28.

Dielectric Increments

Dielectric increment $\Delta\varepsilon_i$ calculations were done with classical molecular dynamics simulations, as discussed in previous publications.[65,69,70] For a the total dipole moment $\mathbf{p}$ of the electrolyte system (which includes the contribution from associated salt species if present), ε of the electrolyte can be calculated as follows (neglecting electronic polarizability):

$$\varepsilon = 1 + \frac{\langle \mathbf{p}^2 \rangle - \langle \mathbf{p} \rangle^2}{3 k_\mathrm{B} T V \varepsilon_0} \tag{30}$$

where V is the volume of the electrolyte.

The dipole moment is calculated by summing over the charge q_i of atoms i multiplied by their position $\mathbf{r_i}$:

$$\mathbf{p} = \Sigma q_i \mathbf{r_i} \tag{31}$$

Single salt species (free ions or CIPs) were placed in a box (approximately 0.1 M) with solvent molecules (127 DMC molecules or 122 PC molecules) using PACKMOL.[71] With the GROMACS[72] MD software, these electrolytes were equilibrated first using a Berendsen barostat (NPT).[73] Afterwards, production runs in the NVT ensemble using the velocity rescaling thermostat were undertaken.[74] At least 2 production runs were undertaken per system. CIPs were associated for the duration of the simulation (each at least 10 ns) and from their dipole moment, in addition to the dipole moment of the solvent species, the dielectric constant of the entire electrolyte solution was found. The dielectric constant of the neat solvent solution was subtracted from this value, which was then subsequently divided by the concentration (e.g. 0.1 m) to obtain the dielectric increment per salt species, as appearing in Table 3:

$$\Delta\varepsilon_i = \frac{\varepsilon(m_i) - \varepsilon(m=0)}{m_i} \tag{32}$$

For PC, the CIP was constrained using a Li-P(F_6) distance of 3.8 Å, the value obtained via electronic structure calculation. The partial charge assignments for the DMC molecule were taken from Soetens et al.,[75] while for PC they were generated using Macromodel software.[76] The latter were then subsequently scaled by 1.07 for the neat solvent dielectric constant to match that of experiment. The other parameters for the PC and DMC molecules are taken from the standard OPLS forcefield.[77,78] The parameter files for ClO_4^- and PF_6^- were taken from Doherty et al.[79] and Lopes et al.[80] The Li^+, of a charge of +1, followed the standard OPLS parameters.[77,78]

DSC Measurements

Battery grade lithium hexafluorophosphate ($LiPF_6$) and DMC were purchased from Gotion Inc. and directly transferred under inert atmosphere to an argon glovebox (Vacuum Atmospheres) maintained below 5 ppm water and oxygen. Battery grade PC was purchased from Sigma Alrdrich. Electrolyte samples were prepared inside the glovebox on a moles per kg solvent basis. Differential scanning calorimetry (DSC) measurements of DMC-based electrolytes were performed on a TA Instruments Q1000 DSC equipped with an RCS90 cooling system. 10 μL of electrolyte were hermetically sealed inside DSC pans (TA Instruments T-zero aluminum hermetic pans) inside the glovebox. The DSC was calibrated prior to measurements using an indium metal standard (Sigma Aldrich). Samples were cycled between -40° and 30°C at a ramp rate of 5°C per minute. Each sample was subjected to an initial controlled heat-cool cycle to erase any thermal history prior to the heat cycle from which phase data was extracted. The liquidus was determined as the peak temperature in the melting endotherm during the second heating cycle. Three replicates were run for each electrolyte concentration. For PC-based electrolyte systems, DSC measurements were performed on a Perkin-Elmer DSC-8000 with a liquid-nitrogen cooling system and helium purge gas. The instrument was calibrated using indium and decane standards. 10 μL of electrolyte were hermetically sealed inside DSC pans (Perkin-Elmer aluminum hermetic pans) inside

the glovebox along with ∼1 mg of mesocarbon microbeads (MCMB) purchased from MTI Corporation. MCMBs were added in order to provide a nucleation site to reduce supercooling.[81] PC electrolytes were cycled between 0° and -100°C at a ramp rate of 0.5° C/min, with an isothermal hold at -100°C for 12 hours prior to reheating. Using this method a liquidus was measured for pure PC which was in good agreement with the literature. However no endothermic phenomena indicating melting was observed for $LiPF_6$ containing electrolytes with concentrations as low as 0.1 m.

Results

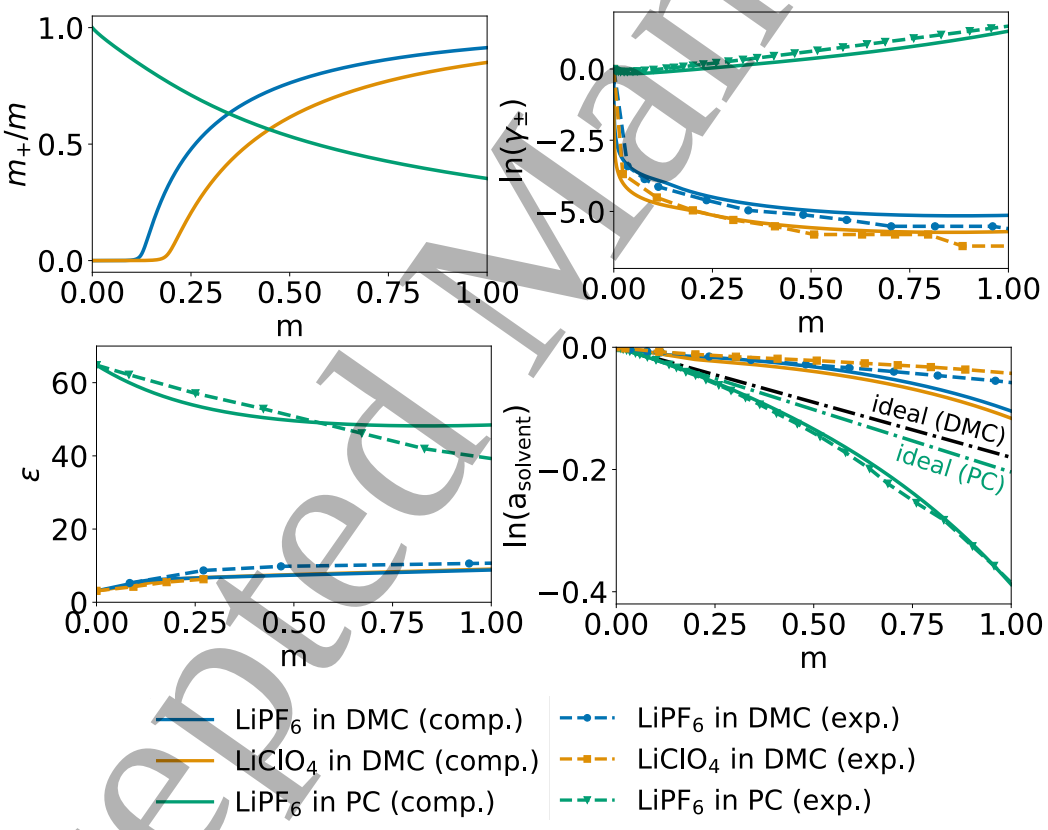

Figure 2: Speciation diagram for different electrolytes (top left). Dielectric constant ε as a function of concentration (bottom left). Logarithm of activity coefficient $\gamma_\pm$ as a function of concentration (top right), shifted by a constant arbitrary value (see text). Logarithm of solvent activity (bottom right). For the bottom left plot, computed data for $LiPF_6$ in DMC overlaps with that of $LiClO_4$ data. Experimental values are taken from literature.[27,39,43,62,82,83]

Figure 2 (top left) shows the calculated speciation diagram. We note that $m_+ = m_-$ and $m_{\mathrm{CIP}} = m - m_+$ due to charge neutrality and mass conservation. $\varepsilon(m)$ is shown as a function of concentration (bottom left). For the DMC-based electrolytes, $\varepsilon(m)$ increases with m, due to the significant CIP fraction and large $\Delta\varepsilon_{\mathrm{CIP}}$. In contrast, for the PC base electrolyte, $\varepsilon(m)$ decreases due to the significant fraction of free ions and very negative cation $\Delta\varepsilon_i$. The trends in speciation and dielectric constant are consistent: the increase in dielectric constant of the low permittivity solvent systems leads to the trend of increase in free ion fraction (DMC systems), a phenomenon known as redissociation.[6,84] This increase in free ion fraction for the DMC-based systems is consistent with the reported molar conductivity increase with increasing concentration.[43,82,85] For the PC-based system, the decrease in dielectric constant with concentration, in addition to the mass action law, promotes a larger fraction of CIPs with increasing salt molality. The computed $\varepsilon(m)$ is larger than that from experiment above ~ 0.5 m, which suggests in this regime the fraction of CIPs is overestimated, and free ion fraction underestimated. We speculate that the moderate disagreement of computed and experimental $\varepsilon(m)$ is due to an overestimation of K_{A}^0 and/or the neglect of more complex solvation effects, such as the concentration dependence of $n_{\mathrm{s},i}$.

Figure 2 (top right) shows $\gamma_\pm$ computed using equations 25 and 26. For DMC-based electrolytes, $\gamma_\pm$ generally decreases with concentration as both the DH and Born effects reduce $\gamma_\pm$ more so than the free solvent loss increases $\gamma_\pm$ (Figure S2). The computed values are shifted by an arbitrary constant value for comparison against experiment in the relevant concentration range, as thermodynamic values are only a function of the derivative of the logarithm of the activity coefficient, and not the absolute values. For the PC-based electrolyte, although the DH effects contribute to a lowering of $\gamma_\pm$, the permittivity decrease leads to an increase in $\gamma_\pm$ due to the Born solvation contribution of the ions. This distinction in behavior for high permittivity (e.g. PC-based) versus low permittivity electrolytes (e.g. DMC-based) also leads to the significant change in the activity of the solvent, shown in the bottom right of Figure 2. The activity of the solvent was directly calculated from the

computed $\gamma_{\pm}$.[20]

For comparison, Figure S3 shows the logarithm of the salt activity coefficients when computed from DH-theory alone[34] using crystallographic radii.[51] Here, the neglect of ion pairing, permittivity effects and free solvent number changes and the use of crystallographic radii leads to incorrect activity coefficients. DH-theory alone predicts a monotonic decrease of activity coefficient with salt concentration. It cannot qualitatively predict that the activity coefficient of $LiPF_6$ salt in PC should increase and severely overestimates the decrease in $\gamma_{\pm}$ with concentration for DMC based electrolytes. This illustrates that DH theory, when used alone, is inadequate to model activity coefficients beyond the dilute limit.

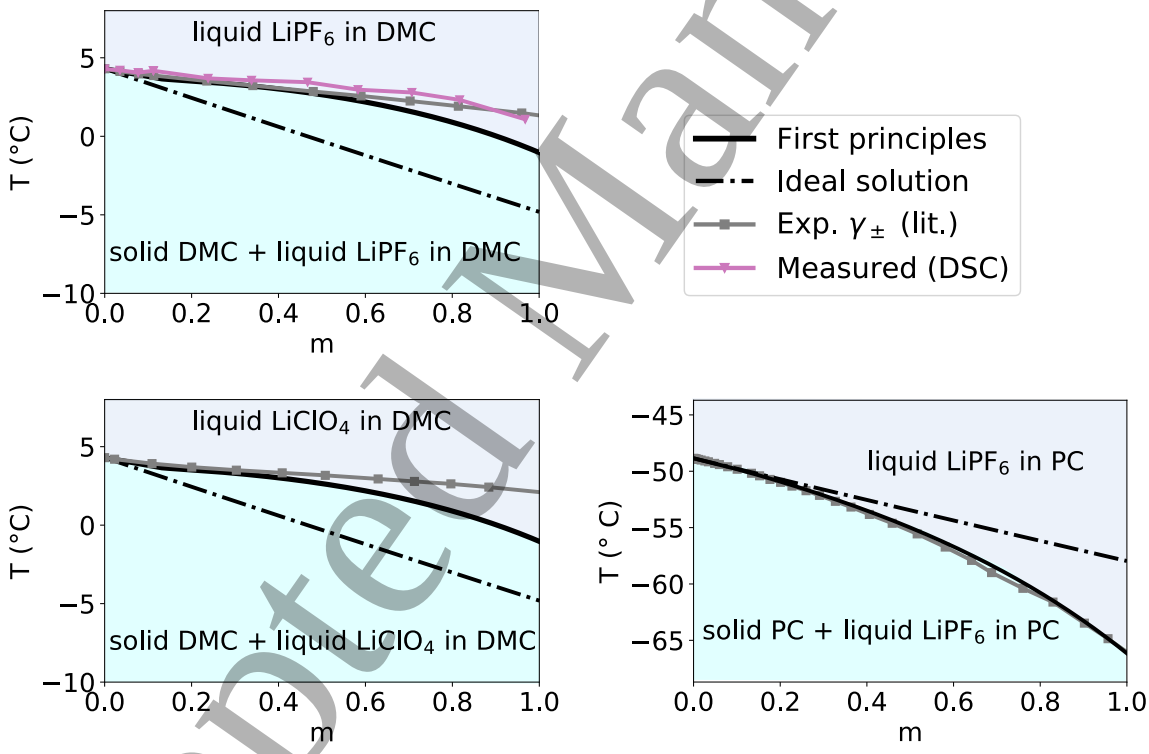

Figure 3: Phase diagrams near the liquidus line for $LiPF_6$ in DMC (top left), $LiClO_4$ in DMC (bottom left) and $LiPF_6$ in PC (bottom right). DSC measurements were carried by the authors, while experimental activity coefficient data used in the calculation of liquidus lines (grey) were taken from literature.[26,27,83,83]

Figure 3 shows the phase diagrams of the various studied electrolytes near the liquidus region from 0 to 1 m. In the top left, $LiPF_6$ in DMC is shown. The values were calculated

following the freezing point depression calculated from equation 1. In the case of ideality, the activity of solvent can be computed assuming an osmotic coefficient of 1.[20] When compared to the ideal (theoretical) solution, the measured and computed liquidus lines are elevated to higher temperatures. This is due to the relatively high activity of the solvent in the DMC electrolyte, as shown in Figure 2. In the bottom left, the phase diagram near the liquidus for $LiClO_4$ in DMC is shown. The result is analogous to $LiPF_6$ in DMC, since both ion pairing and long-range electrostatic interactions are comparable for both systems, given the similarity of the salt. In both DMC-based electrolyte cases, the agreement with experiment is excellent. Furthermore, the phase behavior from DSC data agrees with the computed and experimental $\gamma_{\pm}$ data and shows that the assumptions[19] in deriving equation 1 are reasonable. Moreover, for the $LiPF_6$ in DMC case, the measured liquidus line is in agreement with previous experimental reports.[9] We speculate that the slight disagreement of the computed liquidus line with experiment is due to the neglect of higher order associated salt species beyond CIPs.[43] Higher order aggregates such as neutral salt dimers have been proposed as non-polar,[43] and as such their presence would not be apparent from the measured $\varepsilon(m)$ alone (Figure 2 bottom left). Nonetheless, the agreement between computed and measured $\gamma_{\pm}$ suggests that in this concentration range, consideration of such species may not be needed to accurately model phase behaviour.

For $LiPF_6$ in PC, shown in the bottom right, the behavior vis-a-vis ideality is the opposite: the liquidus lines calculated from experimental and computed activity coefficient data show solution freezing at a lower temperature than that predicted for an ideal solution. This results from the lower solvent activity of the real solution with respect to an ideal solution, as shown in Figure 2. The freezing point depression agreement between liquidus lines calculated from experimental and computed activity coefficient data is once again good. While direct observation of the liquidus of pure PC is possible, direct liquidus line measurements via DSC have proven unsuccessful due to the glass forming nature of PC-based electrolytes.[86,87] We hypothesize that the nucleation and crystallization are inhibited due to kinetic limitations

and that, despite the lack of DSC data, the liquidus line computed from activity coefficient data is theoretically correct, within the assumptions herein. These assumptions include the neglect of the activity coefficient temperature dependence and that the studied concentration range (e.g. above 1 m) is lower than the eutectic composition. Furthermore, we note that the liquidus line in glassy systems such as $LiPF_6$ in PC provides a temperature bound above which there is necessarily a strictly liquid phase. In addition, we also note that the function relating solvent activity to freezing point depression (equation 1) is a function also of the freezing point of the neat solvent. Between various solvents of interest, this can lead to a freezing point depression change on the order of 5°C. For example, the freezing point depression of an ideal DMC-based electrolyte would increase by 3°C at 1 molal if the DMC T_0 was that of PC.

In all cases the enthalpies of fusion and relevant heat capacities used in calculating the liquidus line were measured or found in existing literature (see Table 2 and Methods section). Interestingly, for DMC and PC, these values are comparable, explaining why the ideal (theoretical) liquidus lines show comparable slopes. The results suggest that, provided similar enthalpies of fusion and heat capacities (liquid and solid) of the solvent, high permittivity electrolytes will generally show much greater freezing point depression than low permittivity electrolytes. These findings are expected to play a significant role in the future design of low-temperature LIB electrolytes. Further work on freezing point depression of electrolytes should include the study of different salts in addition to the treatment of ternary electrolytes (e.g. two co-solvents), which are more widely used than binary electrolytes for LIB applications.

Conclusion

In this work a theoretical model to compute activity coefficients and liquidus lines of phase diagrams was elaborated. Within the model, all parameters are computed via density-functional theory electronic structure and classical molecular dynamics simulations. The re-

sults were validated on three carbonate electrolytes, relevant to lithium-ion batteries, showing good to excellent agreement with experiment. Furthermore, beyond the predictive power of the methodology, our work elucidates how human-interpretable physicochemical properties such as ions' radii, ions' solvation number, the concentration-dependent dielectric constant and ion pairing affect the activity coefficients of liquid electrolytes. Finally, we find that high permittivity electrolytes generally show greater freezing point depression than linear carbonate based electrolytes since the former show a dielectric constant decrease with concentration and the latter show a dielectric constant increase with concentration.

Acknowledgements

DSC work at the Molecular Foundry was supported by the Office of Science, Office of Basic Energy Sciences, of the U.S. Department of Energy under Contract No. DE-AC02-05CH11231. We acknowledge support by the Assistant Secretary for Energy Efficiency and Renewable Energy, Vehicle Technologies Office, of the U.S. Department of Energy under Contract DE-AC02-05CH11231, under the Advanced Battery Materials Research (BMR) Program managed by Tien Duong as well as the Low Temperature Electrolyte Program. H.K.B. further acknowledges support from NSF GRFP under Grant no. DGE 1752814. K.D.F is supported by the Berkeley Fellowship for Graduate Study.

References

(1) Ding, M. S.; Xu, K.; Jow, T. R. Liquid-Solid Phase Diagrams of Binary Carbonates for Lithium Batteries. *Journal of The Electrochemical Society* **2000**, *147*, 1688.

(2) Ding, M. S. Liquid-Solid Phase Diagrams of Ternary and Quaternary Organic Carbonates. *Journal of The Electrochemical Society* **2004**, *151*, A731.

(3) Ding, M. S. Liquid-Solid Phase Equilibria and Thermodynamic Modeling for Binary Organic Carbonates. *Journal of Chemical & Engineering Data* **2004**, *49*, 276–282.

(4) Ding, M.; Xu, K.; Jow, T. Phase diagram of EC–DMC binary system and enthalpic determination of its eutectic composition. *Journal of thermal analysis and calorimetry* **2000**, *62*, 177–186.

(5) Ding, M. S. Thermodynamic Analysis of Phase Diagrams of Binary Carbonates Based on a Regular Solution Model. *Journal of The Electrochemical Society* **2002**, *149*, A1063.

(6) Logan, E. R.; Tonita, E. M.; Gering, K. L.; Ma, L.; Bauer, M. K. G.; Li, J.; Beaulieu, L. Y.; Dahn, J. R. A Study of the Transport Properties of Ethylene Carbonate-Free Li Electrolytes. *Journal of The Electrochemical Society* **2018**, *165*, A705–A716.

(7) Petibon, R.; Xia, J.; Ma, L.; Bauer, M. K. G.; Nelson, K. J.; Dahn, J. R. Electrolyte System for High Voltage Li-Ion Cells. *Journal of The Electrochemical Society* **2016**, *163*, A2571–A2578.

(8) Ding, M. S. Excess Gibbs Energy of Mixing for Organic Carbonates from Fitting of Their Binary Phase Diagrams with Nonideal Solution Models. *Journal of Solution Chemistry* **2005**, *34*, 343–359.

(9) Xiong, D. J.; Bauer, M.; Ellis, L. D.; Hynes, T.; Hyatt, S.; Hall, D. S.; Dahn, J. R. Some Physical Properties of Ethylene Carbonate-Free Electrolytes. *Journal of The Electrochemical Society* **2018**, *165*, A126–A131.

(10) Day, R. P.; Xia, J.; Petibon, R.; Rucska, J.; Wang, H.; Wright, A. T. B.; Dahn, J. R. Differential Thermal Analysis of Li-Ion Cells as an Effective Probe of Liquid Electrolyte Evolution during Aging. *Journal of The Electrochemical Society* **2015**, *162*, A2577–A2581.

(11) Xu, K. Nonaqueous Liquid Electrolytes for Lithium-Based Rechargeable Batteries. *Chemical Reviews* **2004**, *104*, 4303–4418.

(12) Xu, K. Electrolytes and Interphases in Li-Ion Batteries and Beyond. *Chemical Reviews* **2014**, *114*, 11503–11618.

(13) Jow, R.; Zhang, S. S.; Xu, K.; Allen, J. Electrolytes for Low Temperature Operations of Li-Ion Batteries. *ECS Transactions* **2007**, *3*, 51–58.

(14) Tan, S.; Shadike, Z.; Hu, E.; Wang, Q.-C.; Yang, X.-Q. Propylene Carbonate-Based Electrolyte for Low Temperature Lithium Batteries. ECS Meeting Abstracts. 2020; p 731, Issue: 4.

(15) Zhang, S.; Xu, K.; Jow, T. The low temperature performance of Li-ion batteries. *Journal of Power Sources* **2003**, *115*, 137–140.

(16) Ringsby, A. J.; Fong, K. D.; Self, J.; Bergstrom, H. K.; McCloskey, B. D.; Persson, K. A. Transport phenomena in low temperature lithium-ion battery electrolytes. *Journal of the Electrochemical Society* **2021**, *168*, 080501.

(17) Collins, G. A.; Geaney, H.; Ryan, K. M. Alternative anodes for low temperature lithium-ion batteries. *Journal of Materials Chemistry A* **2021**,

(18) Li, Q.; Jiao, S.; Luo, L.; Ding, M. S.; Zheng, J.; Cartmell, S. S.; Wang, C.-M.; Xu, K.; Zhang, J.-G.; Xu, W. Wide-temperature electrolytes for lithium-ion batteries. *ACS applied materials & interfaces* **2017**, *9*, 18826–18835.

(19) Ge, X.; Wang, X. Estimation of Freezing Point Depression, Boiling Point Elevation, and Vaporization Enthalpies of Electrolyte Solutions. *Industrial & Engineering Chemistry Research* **2009**, *48*, 2229–2235.

(20) Newman, J.; Thomas-Alyea, K. E. *Electrochemical Systems*; John Wiley & Sons, 2012.

(21) Huckel, E.; Debye, P. Zur theorie der elektrolyte. *Phys. Z* **1923**, *24*, 185–206.

(22) Prentice, G. Electrochemical Engineering. **2003**, Publisher: Elsevier.

(23) Pitzer, K. S. Thermodynamics of electrolytes. I. Theoretical basis and general equations. *The Journal of Physical Chemistry* **1973**, *77*, 268–277, Publisher: ACS Publications.

(24) Pitzer, K. S.; Mayorga, G. Thermodynamics of electrolytes. II. Activity and osmotic coefficients for strong electrolytes with one or both ions univalent. *The Journal of Physical Chemistry* **1973**, *77*, 2300–2308, Publisher: ACS Publications.

(25) Barthel, J.; Neueder, R.; Poepke, H.; Wittmann, H. Osmotic and activity coefficients of nonaqueous electrolyte solutions. 1. Lithium perchlorate in the protic solvents methanol, ethanol, and 2-propanol. *Journal of solution chemistry* **1998**, *27*, 1055–1066, Publisher: Springer.

(26) Barthel, J.; Neueder, R.; Poepke, H.; Wittmann, H. Osmotic coefficients and activity coefficients of nonaqueous electrolyte solutions. Part 2. Lithium perchlorate in the aprotic solvents acetone, acetonitrile, dimethoxyethane, and dimethylcarbonate. *Journal of solution chemistry* **1999**, *28*, 489–503, Publisher: Springer.

(27) Xin, N.; Sun, Y.; Radke, C. J.; Prausnitz, J. M. Osmotic and activity coefficients for five lithium salts in three non–aqueous solvents. *The Journal of Chemical Thermodynamics* **2019**, *132*, 83–92, Publisher: Elsevier.

(28) Blum, L. Mean spherical model for asymmetric electrolytes: I. Method of solution. *Molecular Physics* **1975**, *30*, 1529–1535, Publisher: Taylor & Francis.

(29) Marcus, Y.; Hefter, G. Ion Pairing. *Chemical Reviews* **2006**, *106*, 4585–4621.

(30) Born, M. Volumen und hydratationswärme der ionen. *Zeitschrift für Physik* **1920**, *1*, 45–48, Publisher: Springer.

(31) Atkins, P.; De Paula, J. *Physical Chemistry*, 8th ed.; 2006.

(32) Israelachvili, J. N. *Intermolecular and surface forces*; Academic press, 2011.

(33) De Maeyer, L.; Kessling, G. Ion-solvation and ion-pair equilibria in electrolyte solutions. *Journal of Molecular Liquids* **1995**, *67*, 193–210, Publisher: Elsevier.

(34) Marcus, Y. Ionic Radii in Aqueous Solutions. *Chemical Reviews* **1988**, *88*, 1475–1498.

(35) Buchner, R.; Hefter, G. T.; May, P. M. Dielectric Relaxation of Aqueous NaCl Solutions. *The Journal of Physical Chemistry A* **1999**, *103*, 1–9.

(36) Schlumpberger, S.; Bazant, M. Z. Simple Theory of Ionic Activity in Concentrated Electrolytes. *arXiv:1709.03106 [cond-mat, physics:physics]* **2017**, arXiv: 1709.03106.

(37) Eberspächer, P.; Wismeth, E.; Buchner, R.; Barthel, J. Ion Association of Alkaline and Alkaline-earth Metal Perchlorates in Acetonitrile. *Journal of Molecular Liquids* **2006**, *129*, 3–12.

(38) Guggenheim, E. L. *The specific thermodynamic properties of aqueous solutions of strong electrolytes. The London, Edinburgh, and Dublin Philosophical Magazine and Journal of Science* **1935**, *19*, 588–643.

(39) J. M. Barthel,; Krienke, H.; Kunz, W. *Physical Chemistry of Electrolyte Solutions: Modern Aspects*, springer science & business media ed.; 1998; Vol. 5.

(40) Maribo-Mogensen, B.; Kontogeorgis, G. M.; Thomsen, K. Comparison of the Debye–Hückel and the Mean Spherical Approximation Theories for Electrolyte Solutions. *Industrial & Engineering Chemistry Research* **2012**, *51*, 5353–5363.

(41) Crothers, A. R.; Radke, C. J.; Prausnitz, J. M. *110th Anniversary* : Theory of Activity Coefficients for Lithium Salts in Aqueous and Nonaqueous Solvents and in Solvent Mixtures. *Industrial & Engineering Chemistry Research* **2019**, *58*, 18367–18377.

(42) Gering, K. L. Prediction of Electrolyte Conductivity: Results from a Generalized Molecular Model Based on Ion Solvation and a Chemical Physics Framework. *Electrochimica Acta* **2017**, *225*, 175–189.

(43) Delsignore, M.; Farber, H.; Petrucci, S. Ionic conductivity and Microwave Dielectric Relaxation of Lithium Hexafluoroarsenate (LiAsF6) and Lithium Perchlorate (LiClO4) in Dimethyl Carbonate. *The Journal of Physical Chemistry* **1985**, *89*, 4968–4973.

(44) Simonin, J.-P.; Blum, L.; Turq, P. Real Ionic Solutions in the Mean Spherical Approximation. 1. Simple Salts in the Primitive Model. *The Journal of Physical Chemistry* **1996**, *100*, 7704–7709.

(45) Simonin, J.-P.; Bernard, O.; Blum, L. Real Ionic Solutions in the Mean Spherical Approximation. 3. Osmotic and Activity Coefficients for Associating Electrolytes in the Primitive Model. *The Journal of Physical Chemistry B* **1998**, *102*, 4411–4417.

(46) Self, J.; Fong, K. D.; Persson, K. A. Transport in Superconcentrated $LiPF_6$ and $LiBF_4$ /Propylene Carbonate Electrolytes. *ACS Energy Letters* **2019**, *4*, 2843–2849.

(47) Pliego, J. R.; Riveros, J. M. The Cluster-Continuum Model for the Calculation of the Solvation Free Energy of Ionic Species. *The Journal of Physical Chemistry A* **2001**, *105*, 7241–7247.

(48) Marcus, Y. *Ion Solvation*; John Wiley & Sons Limited, 1986.

(49) Ue, M. Mobility and Ionic Association of Lithium Salts in a Propylene Carbonate-Ethyl Methyl Carbonate Mixed Solvent. *Journal of The Electrochemical Society* **1995**, *142*, 2577.

(50) Schmid, R.; Miah, A. M.; Sapunov, V. N. A new table of the thermodynamic quantities of ionic hydration: values and some applications (enthalpy–entropy compensation and Born radii). *Physical Chemistry Chemical Physics* **2000**, *2*, 97–102.

(51) Ue, M. Mobility and ionic association of lithium and quaternary ammonium salts in propylene carbonate and γ-butyrolactone. *Journal of the electrochemical society* **1994**, *141*, 3336–3342.

(52) Ue, M. Mobility and Ionic Associationof Lithiumand Quaternary Ammonium Salts in Propylene Carbonate and /-Butyrolactone. *J. Electrochem. Soc.* **1994**, *141*, 7.

(53) Tomasi, J.; Mennucci, B.; Cammi, R. Quantum Mechanical Continuum Solvation Models. *Chemical Reviews* **2005**, *105*, 2999–3094.

(54) Self, J.; Fong, K. D.; Logan, E. R.; Persson, K. A. Ion Association Constants for Lithium Ion Battery Electrolytes from First-Principles Quantum Chemistry. *Journal of The Electrochemical Society* **2019**, *166*, A3554–A3558.

(55) Cox, S. J.; Mandadapu, K. K.; Geissler, P. L. Quadrupole-mediated dielectric response and the charge-asymmetric solvation of ions in water. *arXiv preprint arXiv:2103.12389* **2021**,

(56) Nie, M.; Abraham, D. P.; Seo, D. M.; Chen, Y.; Bose, A.; Lucht, B. L. Role of Solution Structure in Solid Electrolyte Interphase Formation on Graphite with $LiPF_6$ in Propylene Carbonate. *The Journal of Physical Chemistry C* **2013**, *117*, 25381–25389.

(57) Seo, D. M.; Reininger, S.; Kutcher, M.; Redmond, K.; Euler, W. B.; Lucht, B. L. Role of Mixed Solvation and Ion Pairing in the Solution Structure of Lithium Ion Battery Electrolytes. *The Journal of Physical Chemistry C* **2015**, *119*, 14038–14046.

(58) Bogle, X.; Vazquez, R.; Greenbaum, S.; Cresce, A. v. W.; Xu, K. Understanding Li^+–Solvent Interaction in Nonaqueous Carbonate Electrolytes with ^{17}O NMR. *The Journal of Physical Chemistry Letters* **2013**, *4*, 1664–1668.

(59) Kondo, K.; Sano, M.; Hiwara, A.; Omi, T.; Fujita, M.; Kuwae, A.; Iida, M.; Mogi, K.;

Yokoyama, H. Conductivity and Solvation of Li^+ Ions of $LiPF_6$ in Propylene Carbonate Solutions. *The Journal of Physical Chemistry B* **2000**, *104*, 5040–5044.

(60) Skarmoutsos, I.; Ponnuchamy, V.; Vetere, V.; Mossa, S. Li^+ Solvation in Pure, Binary, and Ternary Mixtures of Organic Carbonate Electrolytes. *The Journal of Physical Chemistry C* **2015**, *119*, 4502–4515.

(61) Borodin, O.; Olguin, M.; Ganesh, P.; Kent, P. R. C.; Allen, J. L.; Henderson, W. A. Competitive lithium solvation of linear and cyclic carbonates from quantum chemistry. *Physical Chemistry Chemical Physics* **2016**, *18*, 164–175.

(62) Hwang, S.; Kim, D.-H.; Shin, J. H.; Jang, J. E.; Ahn, K. H.; Lee, C.; Lee, H. Ionic Conduction and Solution Structure in $LiPF_6$ and $LiBF_4$ Propylene Carbonate Electrolytes. *The Journal of Physical Chemistry C* **2018**, *122*, 19438–19446.

(63) Payne, R.; Theodorou, I. E. Dielectric properties and relaxation in ethylene carbonate and propylene carbonate. *The Journal of Physical Chemistry* **1972**, *76*, 2892–2900.

(64) Chai, J.-D.; Head-Gordon, M. Long-range Corrected Hybrid Density Functionals with Damped Atom-Atom Dispersion Corrections. *Physical Chemistry Chemical Physics* **2008**, *10*, 6615.

(65) Self, J.; Hahn, N. T.; Fong, K. D.; McClary, S. A.; Zavadil, K. R.; Persson, K. A. Ion Pairing and Redissociaton in Low-Permittivity Electrolytes for Multivalent Battery Applications. *The Journal of Physical Chemistry Letters* **2020**, *11*, 2046–2052.

(66) Cancès, E.; Mennucci, B.; Tomasi, J. A new integral equation formalism for the polarizable continuum model: Theoretical background and applications to isotropic and anisotropic dielectrics. *The Journal of Chemical Physics* **1997**, *107*, 3032–3041.

(67) Ribeiro, R. F.; Marenich, A. V.; Cramer, C. J.; Truhlar, D. G. Use of Solution-Phase

Vibrational Frequencies in Continuum Models for the Free Energy of Solvation. *The Journal of Physical Chemistry B* **2011**, *115*, 14556–14562.

(68) Luchini, G.; Alegre-Requena, J. V.; Funes-Ardoiz, I.; Paton, R. S. GoodVibes: automated thermochemistry for heterogeneous computational chemistry data. *F1000Research* **2020**, *9*, 291.

(69) Self, J.; Wood, B. M.; Rajput, N. N.; Persson, K. A. The Interplay between Salt Association and the Dielectric Properties of Low Permittivity Electrolytes: The Case of $LiPF_6$ and $LiAsF_6$ in Dimethyl Carbonate. *The Journal of Physical Chemistry C* **2018**, *122*, 1990–1994.

(70) Hahn, N. T.; Self, J.; Seguin, T. J.; Driscoll, D. M.; Rodriguez, M. A.; Balasubramanian, M.; Persson, K. A.; Zavadil, K. R. The critical role of configurational flexibility in facilitating reversible reactive metal deposition from borohydride solutions. *Journal of Materials Chemistry A* **2020**, *8*, 7235–7244.

(71) Martínez, L.; Andrade, R.; Birgin, E. G.; Martínez, J. M. PACKMOL: A Package for Building Initial Configurations for Molecular Dynamics Simulations. *Journal of Computational Chemistry* **2009**, *30*, 2157–2164.

(72) Abraham, M. J.; Murtola, T.; Schulz, R.; Páll, S.; Smith, J. C.; Hess, B.; Lindahl, E. GROMACS: High Performance Molecular Simulations Through Multi-Level Parallelism from Laptops to Supercomputers. *SoftwareX* **2015**, *1-2*, 19–25.

(73) Berendsen, H. J. C.; Postma, J. P. M.; van Gunsteren, W. F.; DiNola, A.; Haak, J. R. Molecular Dynamics with Coupling to an External Bath. *The Journal of Chemical Physics* **1984**, *81*, 3684–3690.

(74) Bussi, G.; Donadio, D.; Parrinello, M. Canonical Sampling Through Velocity Rescaling. *The Journal of Chemical Physics* **2007**, *126*, 014101.

(75) Soetens, J.-C.; Millot, C.; Maigret, B. Molecular Dynamics Simulation of LiBF4 in Ethylene Carbonate, Propylene Carbonate and Dimethyl Carbonate solvents. *The Journal of Physical Chemistry A* **1998**, *102*.

(76) Schröder, C.; Rudas, T.; Steinhauser, O. Simulation studies of ionic liquids: Orientational correlations and static dielectric properties. *The Journal of Chemical Physics* **2006**, *125*, 244506.

(77) Jorgensen, W. L. Free energy calculations: a breakthrough for modeling organic chemistry in solution. *Accounts of Chemical Research* **1989**, *22*, 184–189.

(78) Jorgensen, W. L.; Maxwell, D. S.; Tirado-Rives, J. Development and Testing of the OPLS All-Atom Force Field on Conformational Energetics and Properties of Organic Liquids. *Journal of the American Chemical Society* **1996**, *118*, 11225–11236.

(79) Doherty, B.; Zhong, X.; Gathiaka, S.; Li, B.; Acevedo, O. Revisiting OPLS Force Field Parameters for Ionic Liquid Simulations. *Journal of Chemical Theory and Computation* **2017**, *13*, 6131–6145.

(80) Canongia Lopes, J. N.; Deschamps, J.; Pádua, A. A. H. Modeling Ionic Liquids Using a Systematic All-Atom Force Field. *The Journal of Physical Chemistry B* **2004**, *108*, 2038–2047.

(81) Ding, S.; Xu, K.; Zhang, S.; Jow, T.; Amine, K.; Henriksen, G. Diminution of supercooling of electrolytes by carbon particles. *Journal of the Electrochemical Society* **1999**, *146*, 3974, Publisher: IOP Publishing.

(82) Lee, H.; Hwang, S.; Kim, M.; Kwak, K.; Lee, J.; Han, Y.-K.; Lee, H. Why Does Dimethyl Carbonate Dissociate Li Salt Better Than Other Linear Carbonates? Critical Role of Polar Conformers. *The Journal of Physical Chemistry Letters* **2020**, *11*, 10382–10387, Publisher: ACS Publications.

(83) Stewart, S.; Newman, J. Measuring the salt activity coefficient in lithium-battery electrolytes. *Journal of The Electrochemical Society* **2008**, *155*, A458, Publisher: IOP Publishing.

(84) Petrucci, S.; Masiker, M. C.; Eyring, E. M. The Possible Presence of Triple Ions in Electrolyte Solutions of Low Dielectric Permittivity. *Journal of Solution Chemistry* **2008**, *37*, 1031–1035.

(85) Doucey, L.; Revault, M.; Lautié, A.; Chaussé, A.; Messina, R. A study of the Li/Li+ couple in DMC and PC solvents: Part 1: Characterization of LiAsF6/DMC and LiAsF6/PC solutions. *Electrochimica acta* **1999**, *44*, 2371–2377.

(86) Ding, M. S. Electrolytic Conductivity and Glass Transition Temperature as Functions of Salt Content, Solvent Composition, or Temperature for $LiPF_6$ in Propylene Carbonate + Diethyl Carbonate. *Journal of Chemical & Engineering Data* **2003**, *48*, 519–528.

(87) Szklarz, G.; Adrjanowicz, K.; Paluch, M. Cooling-Rate versus Compression-Rate Dependence of the Crystallization in the Glass-Forming Liquid, Propylene Carbonate. *Crystal Growth & Design* **2018**, *18*, 2538–2544.